Electronic Supplementary Material (ESI) for Nanoscale.

Electronic Supplementary Information†

Polydopamine-based concentric nanoshells with programmable architectures and plasmonic properties

Chun Kit K. Choi,‡[a] Xiaolu Zhuo,‡[b] Yee Ting Elaine Chiu,[a] Hongrong Yang,[a] Jianfang Wang,[b] and Chung Hang Jonathan Choi*[a,c]

[a]*Department of Biomedical Engineering,* [b]*Department of Physics,* [c]*Shun Hing Institute of Advanced Engineering, The Chinese University of Hong Kong, Shatin, New Territories, Hong Kong, China*

‡*These authors contributed equally to this work.*

**To whom correspondence should be addressed. E-mail: jchchoi@cuhk.edu.hk.*

Supporting Figures and Tables

Sample	(a) Nanoshells		(b) Nanomatryoshkas				(c) Concentric nanoshells		
	PDA @Au NP	PDA @Ag NP	Au @PDA @Au NP	Ag @PDA @Ag NP	Au @PDA @Ag NP	Ag @PDA @Au NP	PDA @Au @PDA @Au NP	PDA @Au @PDA @Ag NP	Au @PDA @Au @PDA @Au NP
Internal radii (nm)	$[r_1, r_2]$= [55, 75]		$[r_1, r_2, r_3]$= [20, 50, 70]				$[r_1, r_2, r_3, r_4]$= [55, 75, 105, 125]		$[r_1, r_2, r_3, r_4, r_5]$= [20, 50, 70, 100, 120]

Table S1 Fixed internal radii of PDA-based plasmonic (a) nanoshells, (b) nanomatryoshkas, and (c) concentric nanoshells employed for simulating their extinction spectra by finite difference time domain (FDTD) calculations.

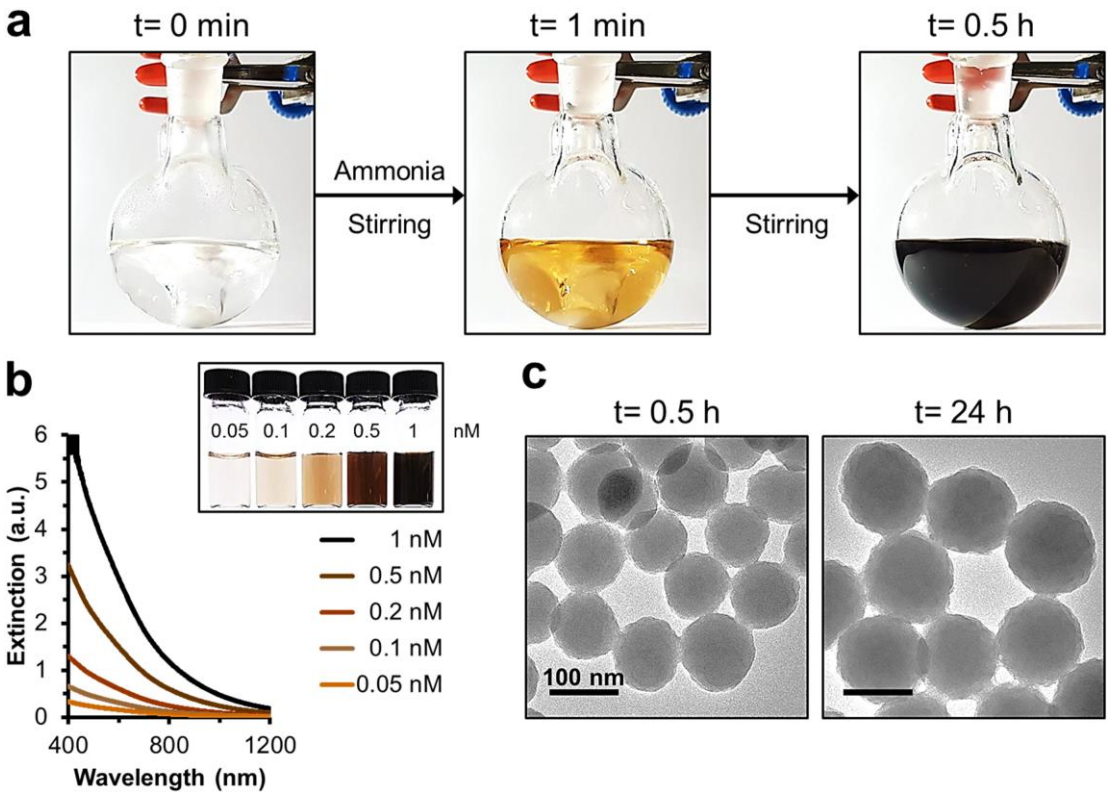

Fig. S1 Synthesis and characterization of polydopamine nanoparticles (PDA NPs) used as unconventional dielectric cores. (a) Evolution of the color of dopamine monomers dispersed in a mixed water-ethanol solvent upon the addition of ammonia as the catalyst. (b) Extinction spectra of aqueous PDA NP solutions at different concentrations. Regardless of the concentration, PDA NPs do not exhibit any extinction peak in the spectral range of 400–1200 nm. Inset: Color of PDA NPs at each indicated concentration (in nM). (c) Transmission electron microscopic (TEM) images of the as-synthesized PDA NPs obtained after 0.5 h (left) and 24 h (right) of stirring. We observed a significant size reduction of the resultant PDA NPs by shortening the polymerization time of dopamine monomers. By dynamic light scattering (DLS) measurements, hydrodynamic diameter of the PDA NPs obtained at 0.5 h and 24 h is 126.2 ± 2.0 nm and 179.2 ± 1.9 nm, respectively (Table S2).

Polymer-ization time (h)	Physical diameter (nm)[a]	Hydro-dynamic diameter (PDI) (nm)[b]	Concen-tration (nM)[c]	Zeta potential (pH= 7.0) (mV)[b]	Zeta potential (pH= 3.0) (mV)[b]
0.5	103.1 ± 8.3	126.2 ± 2.0 (0.043)	1	−22.77 ± 2.27	+19.17 ± 2.67
24	133.6 ± 3.4	179.2 ± 1.9 (0.051)	1.5	−38.02 ± 1.12	+24.56 ± 0.89

Table S2 Physicochemical characterization of PDA NPs obtained after 0.5 and 24 h of polymerization. [a]Values were obtained from the analysis of over 100 NPs in multiple TEM images by the ImageJ software. Results are given in mean ± SD. [b]Measured by the ZetaPlus zeta potential and particle size analyzer. Results are given in mean ± SD of 10 measurements. Numeral in bracket indicates polydispersity index (PDI). [c]Measured by nanoparticle tracking analysis using NanoSight.

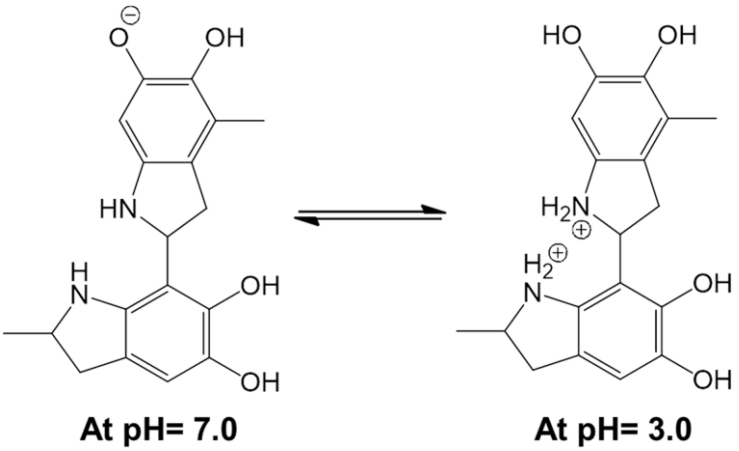

Fig. S2 pH-tunable surface charge of PDA NPs. The chemical structure of PDA NPs at different pH values illustrates the change in the protonation state of functional groups on the surface of PDA NPs.[1,2]

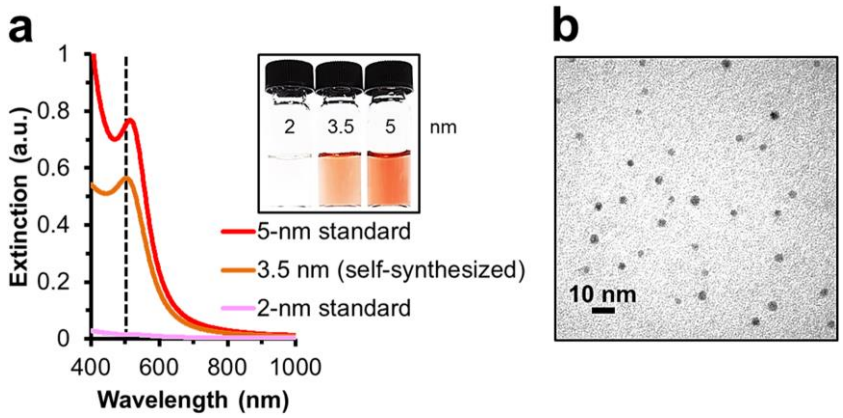

Fig. S3 Characterization of Au seed colloids. (a) Extinction spectra of our as-synthesized Au seed colloids of ~3.5 nm in diameter and commercially available 2-nm and 5-nm Au colloids (Ted Pella, USA). The surface plasmon resonance peak (λ_{spr}) of the 3.5-nm seeds is located at 503 nm between the peaks of the 2-nm Au colloids at ~500 nm (not clearly visible due to their low extinction) and the 5-nm Au colloids at 514 nm. This indicates that the typical size of our Au seeds is within 2 to 5 nm, in agreement with a previous report.[3] Inset: Color of the 2-nm, 3.5-nm, and 5-nm Au colloids. (b) A high-magnification TEM image of the 3.5-nm Au seeds.

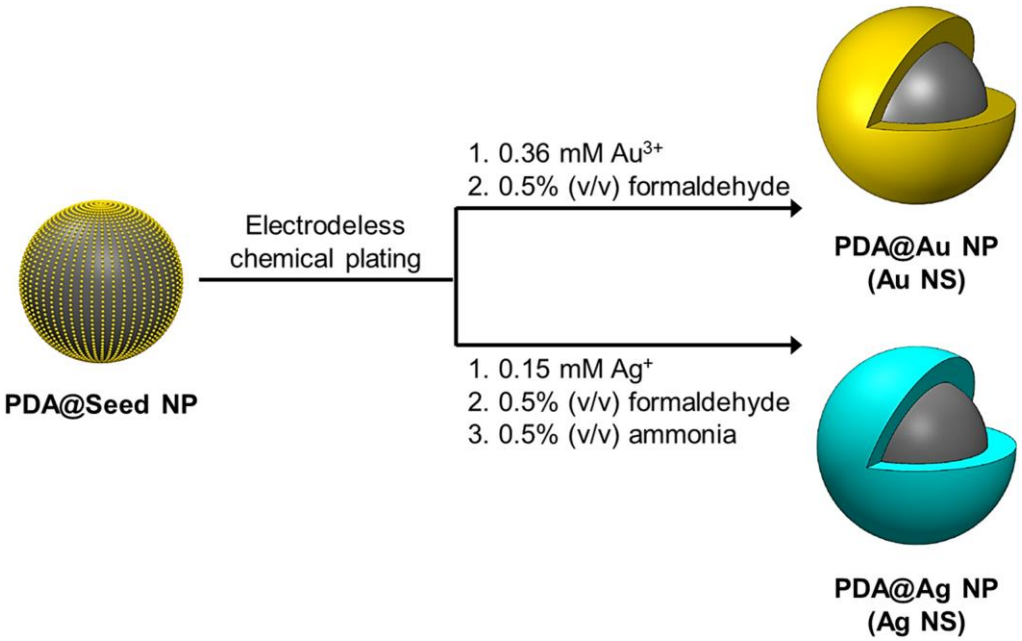

Fig. S4 Schematic illustration of constructing PDA-based gold nanoshells (Au NSs or PDA@Au NPs) and silver nanoshells (Ag NSs or PDA@Ag NPs). Starting from the PDA NPs densely decorated with Au seed colloids (PDA@Seed NPs) (Fig. 2c of the main text), we can fabricate PDA-based Au NSs and Ag NSs (Fig. 2d and Fig. 4a of the main text) via the conventional electrodeless chemical plating. Note that the growth of Ag NS requires extra addition of ammonia (as the catalyst) besides formaldehyde (as the reducing agent).[4]

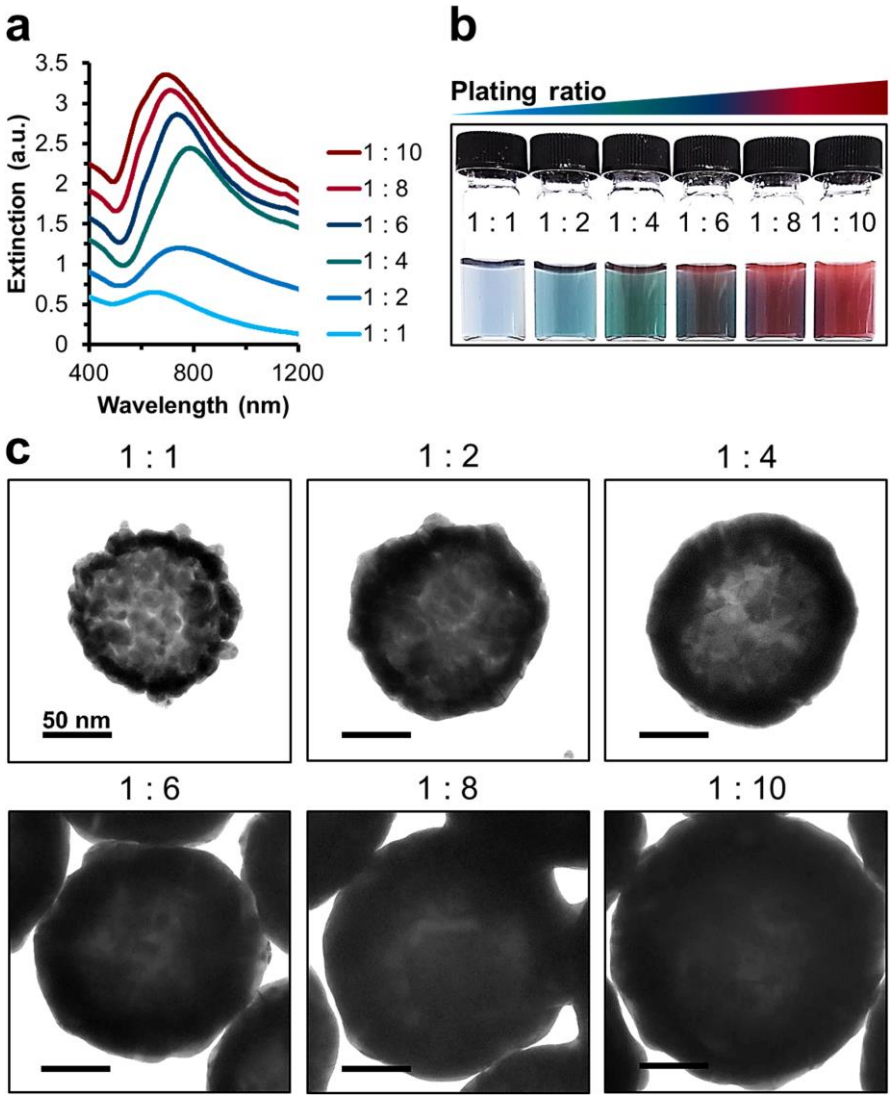

Fig. S5 Monitoring of the growth of a single layer of Au NS onto the surface of PDA NPs. (a) Extinction spectra of PDA@Au NPs obtained by using different plating ratios, i.e., volume ratio between the seeded PDA NPs (PDA@Seed NPs) and the plating solution. (b) Color of PDA@Au NPs obtained by using different plating ratios. (c) Single-particle TEM images of PDA@Au NPs obtained by using different plating ratios clearly show the coalescence of the immobilized Au seed colloids on the PDA NP surface to form a complete and smooth Au NS when the plating ratio reaches 1 : 4. Further increasing the plating ratio results in the overgrowth of Au NS, in agreement with the gradual blue-shift of the λ_{spr} as shown in (a).

Surface plasmon resonance peak (nm)	**Internal radii [r_1, r_2] (nm)[a]**	**Physical diameter (nm)[a]**	**Hydrodynamic diameter (PDI) (nm)[b]**
779	[59.0 ± 6.6, 80.5 ± 7.1]	156.0 ± 12.6	150.4 ± 2.5 (0.143)

Table S3 Physicochemical characterization of the optimized PDA-based Au NSs (PDA@Au NPs). [a]Values were obtained from the analysis of over 100 NPs in multiple TEM images by the ImageJ software. Results are given in mean ± SD. The physical dimension of the optimized Au NSs is represented by [r_1, r_2],[5] where r_1 indicates the radius of the PDA core and r_2 indicates the radius of the whole PDA@Au NP. [b]Measured by the ZetaPlus zeta potential and particle size analyzer. Results are given in mean ± SD of 10 measurements. Numeral in bracket indicates PDI.

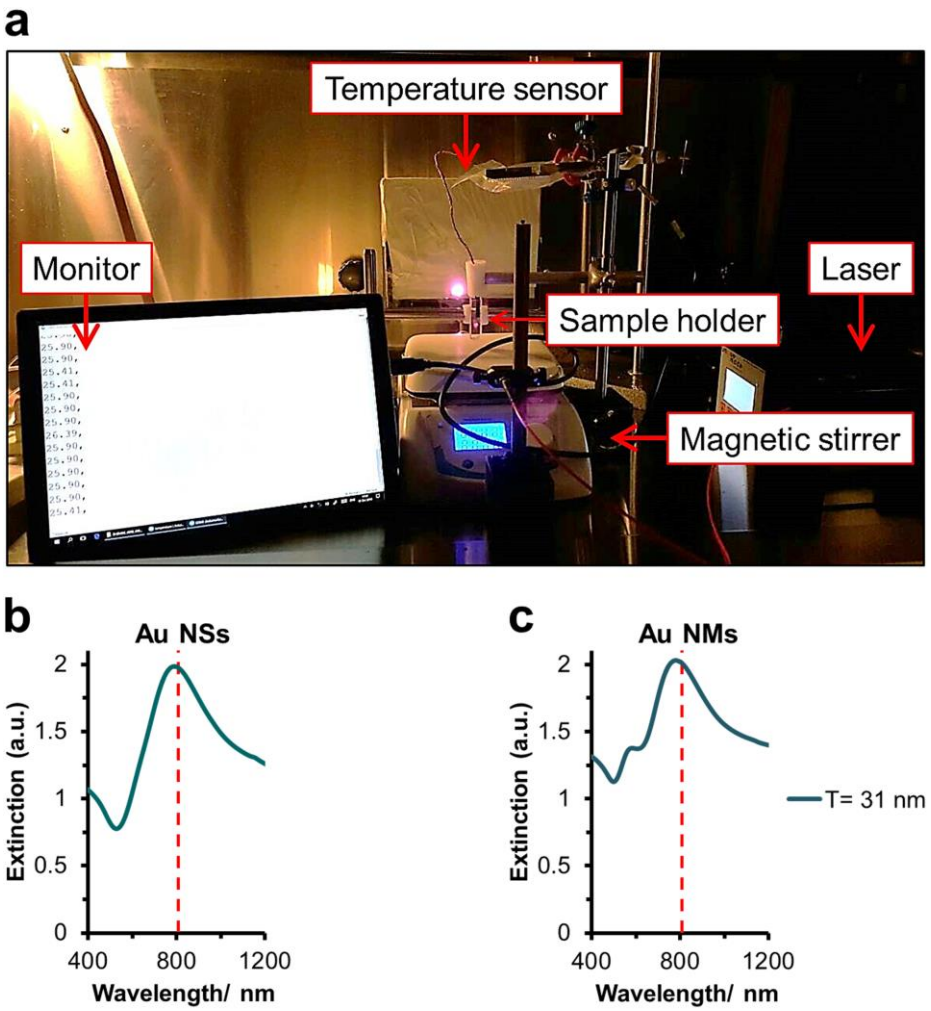

Fig. S6 Photothermal response of PDA-based Au nanoshells (Au NSs) and Au nanomatryoshkas (Au NMs). (a) Custom-built experimental set-up for conducting photothermal studies of PDA-based Au NSs and Au NMs depicted in Fig. 2g and Fig. 3e of the main text. We irradiated both samples by using an 809-nm laser operating at a power intensity of 4 W/cm^2. Extinction spectra of the as-synthesized (b) Au NSs (PDA@Au NPs, $OD_{809\ nm}$= 2) and (c) Au NMs (Au@PDA@Au NPs, $OD_{809\ nm}$= 2) with an interior nanogap thickness (denoted as "T") of 31 nm.

Sample	Surface plasmon resonance peak (nm)	Physical diameter (nm)[a]	Hydrodynamic diameter (PDI) (nm)[b]	Zeta potential (mV)[b]
Au NPs	525	39.07 ± 2.30	42.6 ± 0.6 (0.097)	−37.06 ± 2.60
Au@PEG NPs	527	39.07 ± 2.30	57.4 ± 0.5 (0.071)	−28.43 ± 0.95

Table S4 Physicochemical characterization of the Au cores employed for the synthesis of PDA-based NMs. [a]Values were obtained from the analysis of over 100 NPs in multiple TEM images by the ImageJ software. Results are given in mean ± SD. [b]Measured by the ZetaPlus zeta potential and particle size analyzer. Results are given in mean ± SD of 10 measurements. Numeral in bracket indicates PDI.

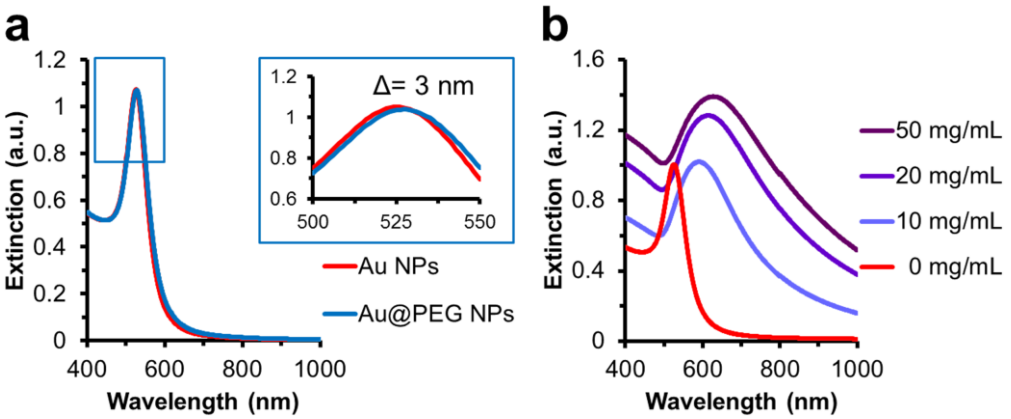

Fig. S7 PEGylation of gold nanoparticles (Au NPs) of ~40 nm in diameter for preventing salt-induced aggregation during the coating of PDA shell. (a) Extinction spectra of Au NPs before (red) and after (blue) PEGylation under continuous sonication for 1 h. Typically, the λ_{spr} of Au NPs exhibits a 3-nm red-shift (Δ) from 525 nm to 528 nm upon complete PEGylation. (b) Extinction spectra of Au@PDA NPs obtained by polymerizing different initial dopamine concentrations with Au@PEG NPs to form the PDA shell under continuous sonication for 1 h. Our results show that PEGylation can afford coating of PDA shell onto Au NPs at very high dopamine concentrations (i.e., from 10 to 50 mg/mL) without causing significant aggregation of the resultant Au@PDA NPs,[6,7] as evidenced by the single sharp peaks.

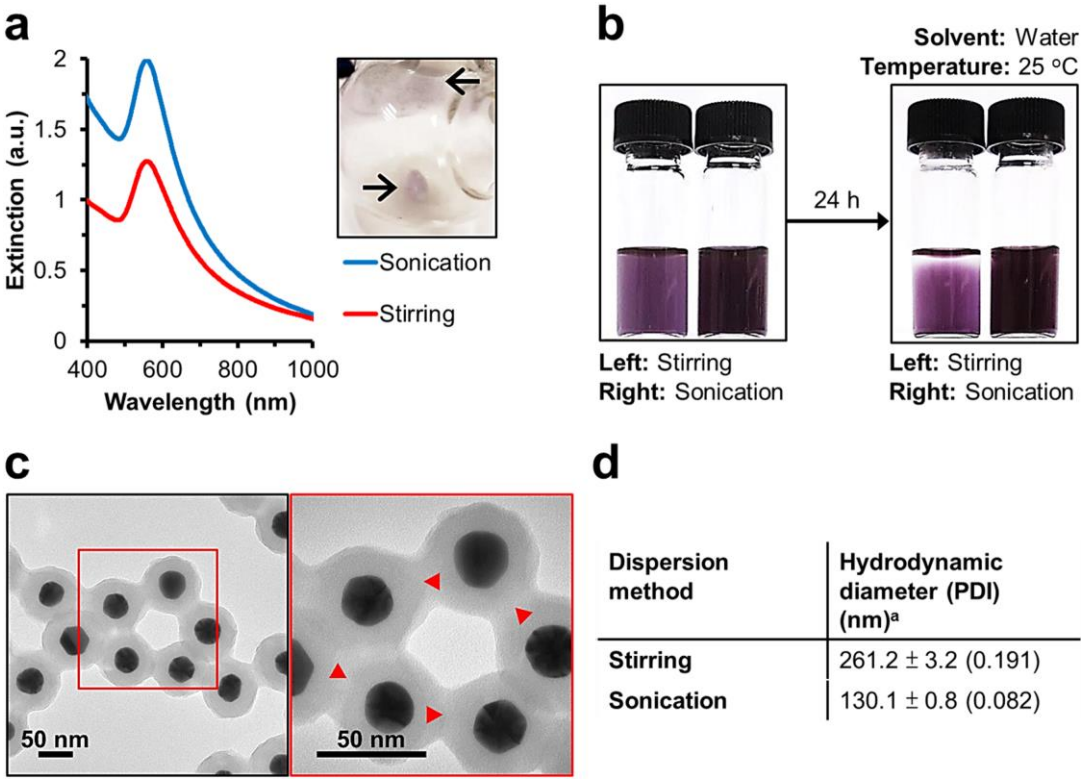

Dispersion method	Hydrodynamic diameter (PDI) (nm)[a]
Stirring	261.2 ± 3.2 (0.191)
Sonication	130.1 ± 0.8 (0.082)

Fig. S8 Effect of dispersion method on the synthesis of Au@PDA NPs. (a) Extinction spectra of Au@PDA NPs obtained by reacting Au@PEG NPs with an initial dopamine concentration of 0.5 mg/mL under sonication or stirring for 3 h. The λ_{spr} of the resultant Au@PDA NPs formed by stirring is lower in extinction and slightly broader than that formed by sonication, possibly due to deposition of aggregated NPs on the reaction flask and the stir bar (inset, arrows). (b) Colloidal stability of the as-synthesized Au@PDA NPs in water at room temperature. After 24 h, we observed significant sedimentation of Au@PDA NPs formed by stirring but not those formed by sonication. (c) TEM images of Au@PDA NPs obtained by stirring show clustering of NPs with their PDA shells sticking to each other (triangles). The right panel is a magnified image of the boxed region shown in the left panel. (d) DLS measurements of Au@PDA NPs obtained by the two different dispersion methods. The sample obtained by stirring is more likely to be aggregated than that obtained by sonication, as evidenced by its larger hydrodynamic diameter and PDI. [a]Measured by the ZetaPlus zeta potential and particle size analyzer. Results are given in mean ± SD of 10 measurements. Numeral in bracket indicates PDI.

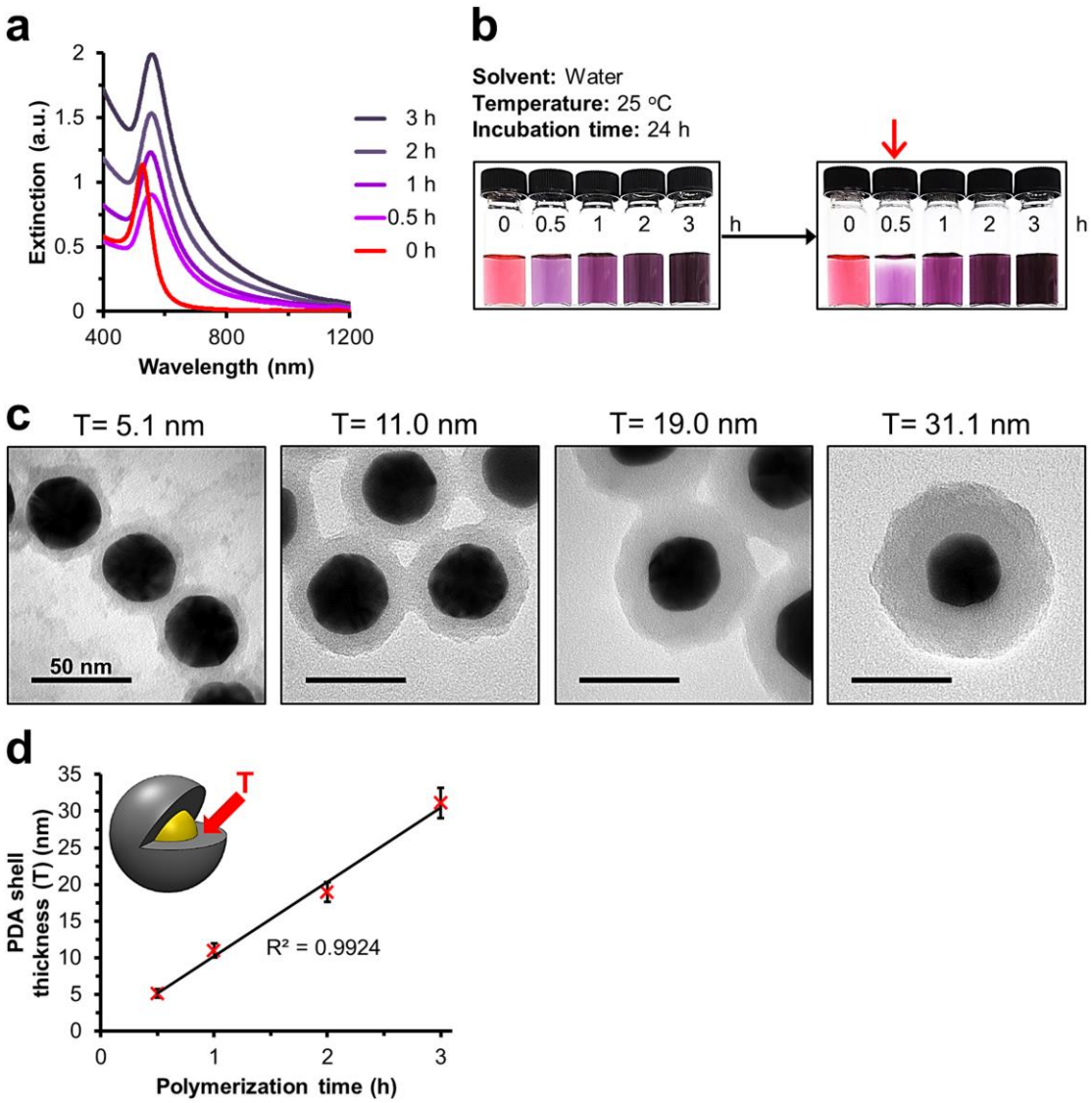

Fig. S9 Optimization of the polymerization time for assembling Au@PDA NPs at a fixed initial dopamine concentration. (a) Extinction spectra of Au@PDA NPs obtained by sonicating Au@PEG NPs in a Tris-buffered dopamine solution (0.5 mg/mL, pH= 8.5) for four different durations of polymerization time. We observed significant peak broadening when Au@PDA NPs are collected at the earlier time points (i.e., 0.5 h and 1 h) but not the later time points (i.e., 2 h and 3 h). (b) Colloidal stability of the as-synthesized Au@PDA NPs in water at room temperature. After 24 h, severe sedimentation occurred only for the sample collected after 0.5 h of polymerization (arrow). Therefore, we chose 3 h as the polymerization time when we tuned the initial dopamine concentration in Fig. 3b of the main text. (c) By TEM imaging, Au@PDA NPs obtained at different time points possess four different PDA shell thicknesses (denoted as "T"). (d) There is a linear relationship between T (in nm) and polymerization time (in h).

Polymer-ization time (h)	Surface plasmon resonance peak (nm)	Au core diameter (nm)[a]	PDA shell thickness (nm)[a]	Physical diameter (nm)[a]	Hydro-dynamic diameter (PDI) (nm)[b]
0.5	555	39.06 ± 1.93	5.12 ± 0.58	50.16 ± 2.73	146.6 ± 2.1 (0.188)
1	554		10.97 ± 0.94	63.71 ± 2.68	109.9 ± 1.0 (0.152)
2	556		18.96 ± 1.33	80.20 ± 3.88	115.5 ± 1.0 (0.122)
3	558		31.10 ± 2.09	99.14 ± 4.07	130.1 ± 0.8 (0.082)

Table S5 Physicochemical characterization of Au@PDA NPs resulting from different durations of polymerization time. The initial dopamine concentration was kept at 0.5 mg/mL. [a]Values were obtained from the analysis of over 100 NPs in multiple TEM images by the ImageJ software. Results are given in mean ± SD. [b]Measured by the ZetaPlus zeta potential and particle size analyzer. Results are given in mean ± SD of 10 measurements. Numeral in bracket indicates PDI. These dynamic light scattering (DLS) data corroborate the UV-vis-NIR spectroscopic results and the TEM images shown in Fig. S9.

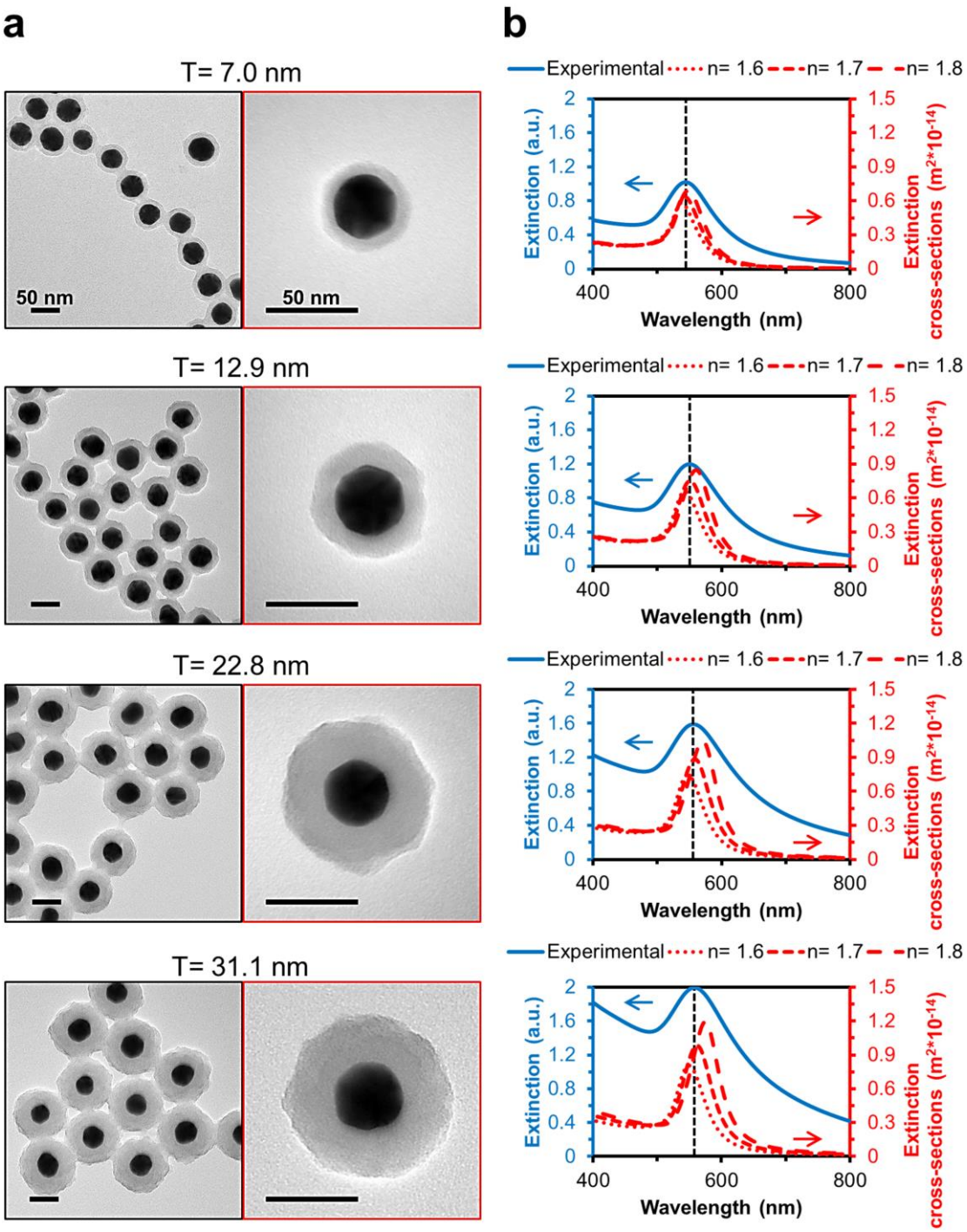

Fig. S10 Characterization of Au@PDA NPs with programmable PDA shell thickness ("T"). (a) Additional TEM images of the optimized Au@PDA NPs with four different values of T corroborate the UV-vis-NIR spectroscopic results, scanning TEM (STEM), and elemental line mapping data featured in Fig. 3b–d of the main text. (b) Experimental and calculated extinction spectra of the optimized Au@PDA NPs with four different values of T. The experimental extinction spectra consistently match with the calculated ones when the refractive index of PDA (n_{PDA}) is set as 1.7 for all four samples.

Initial dopamine concen-tration (mg/mL)	Surface plasmon resonance peak (nm)	Au core diameter (nm)[a]	PDA shell thickness (nm)[a]	Physical diameter (nm)[a]	Hydro-dynamic diameter (PDI) (nm)[b]
0.1	544	39.06 ± 1.93	6.95 ± 0.57	53.31 ± 2.88	61.7 ± 0.3 (0.043)
0.2	550		12.92 ± 0.72	63.56 ± 2.48	77.8 ± 0.4 (0.022)
0.4	556		22.77 ± 1.29	83.36 ± 2.78	104.1 ± 1.1 (0.052)
0.5	558		31.10 ± 2.09	99.14 ± 4.07	130.1 ± 0.8 (0.082)

Table S6 Physicochemical characterization of the optimized Au@PDA NPs with four defined PDA shell thicknesses. [a]Values were obtained from the analysis of over 100 NPs in multiple TEM images by the ImageJ software. Results are given in mean ± SD. [b]Measured by the ZetaPlus zeta potential and particle size analyzer. Results are given in mean ± SD of 10 measurements. Numeral in bracket indicates PDI. These DLS data corroborate the UV-vis-NIR spectroscopic results, STEM, and elemental line mapping data shown in Fig. 3b–d of the main text.

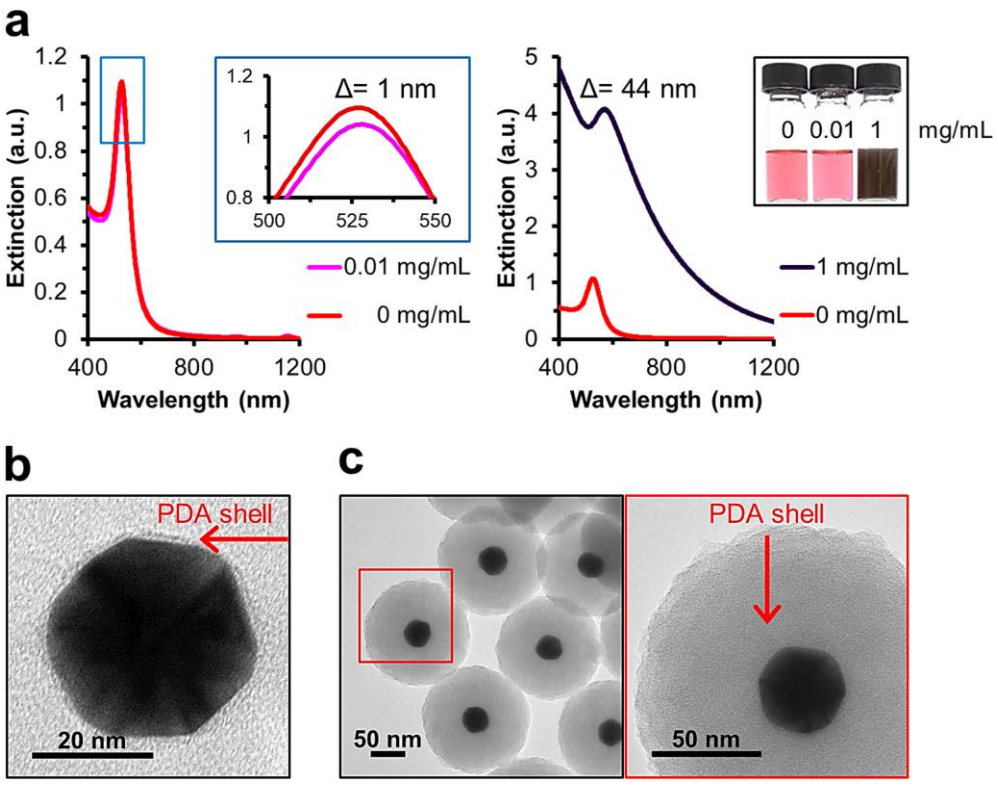

Fig. S11 Characterization of Au@PDA NPs with an ultra-thin or an extremely thick PDA shell. (a) Extinction spectra of Au@PEG NPs after being reacted with 0.01 mg/mL of dopamine for 3 h (left) and 1 mg/mL of dopamine for 6 h (right). The size of Au cores is ~40 nm (Table S4). Inset: Color change of Au@PEG NPs after polymerization of dopamine at the indicated initial concentrations (in mg/mL). Δ represents the red-shift of the λ_{spr} of Au@PEG NPs before and after coating of the PDA shell. (b) TEM image of a Au@PDA NP with an ultra-thin PDA shell of ~1 nm thick. (c) TEM image of Au@PDA NPs with an extremely thick PDA shell of ~60 nm thick. The right panel is a magnified image of the boxed region shown in the left panel.

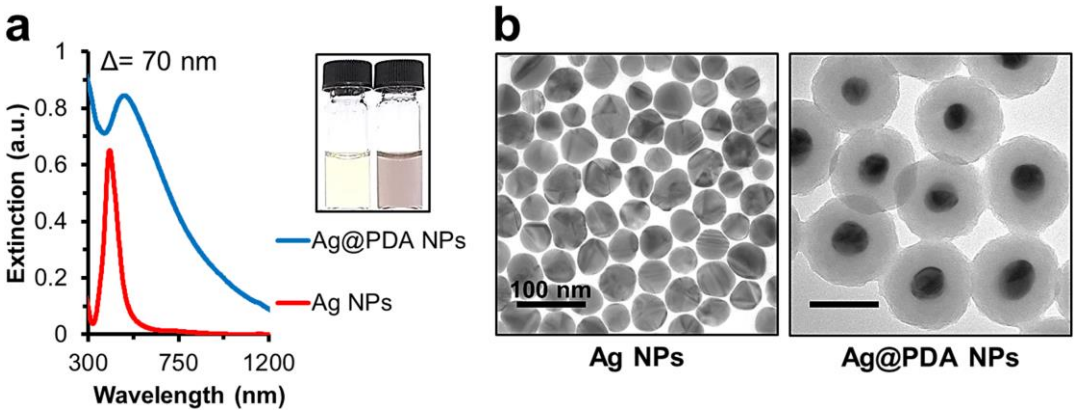

Fig. S12 Characterization of PDA-coated Ag NPs (Ag@PDA NPs). (a) Extinction spectra of Ag NPs of ~40 nm in diameter before (red) and after (after) being reacted with 0.4 mg/mL of dopamine for 6 h upon continuous stirring. Inset: Color change of Ag NPs after coating with a layer of PDA shell. The λ_{spr} of Ag NPs exhibits a 70-nm red-shift (Δ) from 409 nm to 479 nm upon PDA coating. (b) TEM images of Ag NPs before (left) and after (right) deposition of the PDA shell of ~30 nm in thickness onto the surface of Ag cores. Note that the Ag NPs employed in this study show a less homogeneous size distribution (hydrodynamic diameter= 41.0 ± 0.4 nm and PDI= 0.324) than the Au NPs (hydrodynamic diameter= 42.6 ± 0.6 nm and PDI= 0.097).

PDA shell thickness (nm)[a]	**Zeta potential (pH= 7.0) (mV)[b]**	**Zeta potential (pH= 3.0) (mV)[b]**
6.95 ± 0.57	−28.59 ± 7.47	+7.18 ± 0.46
12.92 ± 0.72	−36.06 ± 1.46	+18.94 ± 0.62
22.77 ± 1.29	−28.34 ± 2.38	+22.80 ± 0.90
31.10 ± 2.09	−24.55 ± 1.83	+15.75 ± 0.51

Table S7 pH-tunable surface charge of the optimized Au@PDA NPs with four defined PDA shell thicknesses ("T"). The surface charge of Au@PDA NPs changes from negative (at neutral pH) to positive (at pH= 3.0), regardless of the PDA shell thickness. [a]Values were obtained from the analysis of over 100 NPs in multiple TEM images by the ImageJ software. Results are given in mean ± SD. [b]Measured by the ZetaPlus zeta potential and particle size analyzer. Results are given in mean ± SD of 10 measurements.

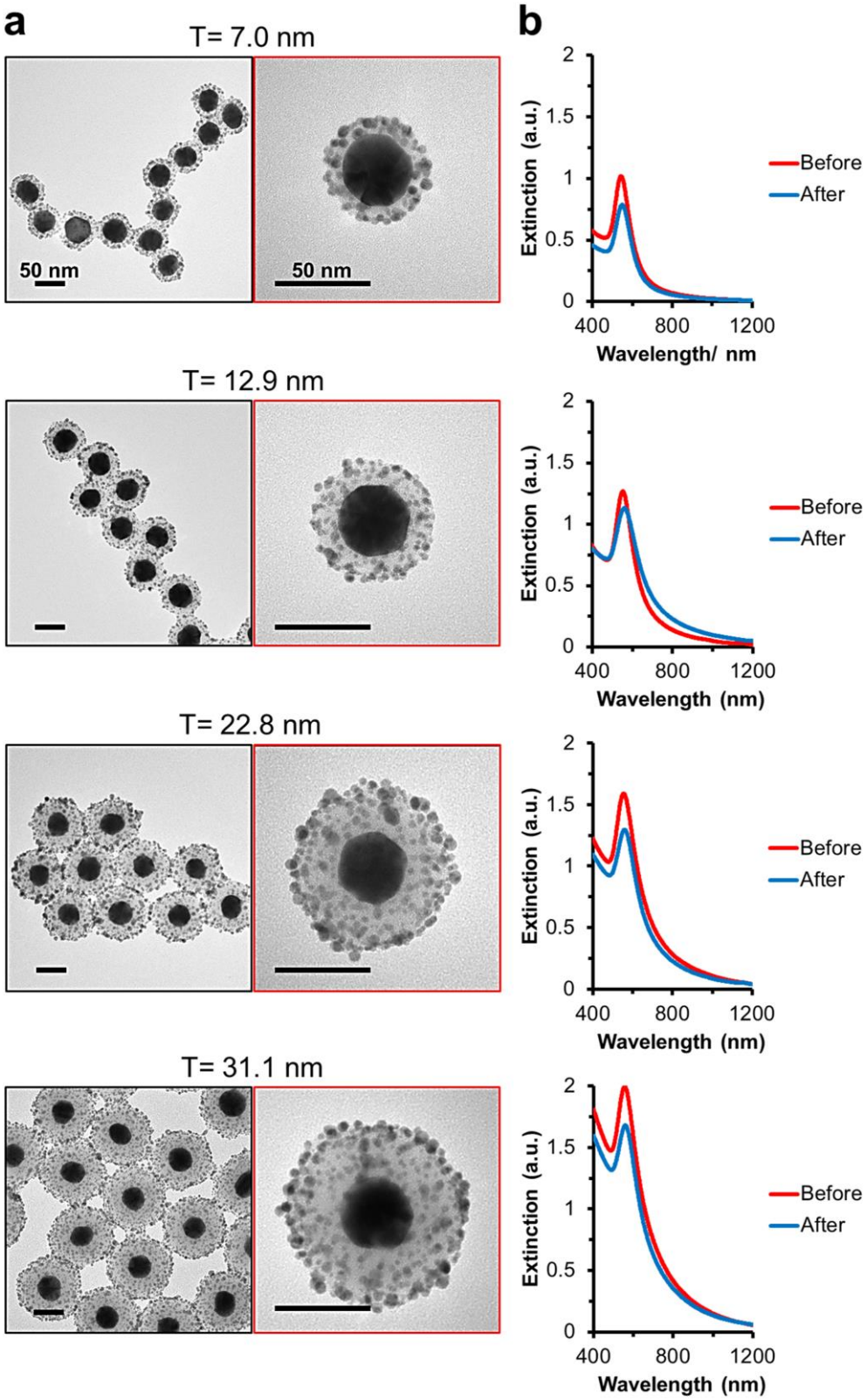

Fig. S13 Characterization of Au@PDA@Seed NPs with four defined PDA shell thicknesses ("T"). (a) TEM images of Au@PDA@Seed NPs with their indicated T values. (b) Extinction spectra of Au@PDA NPs before (red) and after (blue) electrostatic seed immobilization.

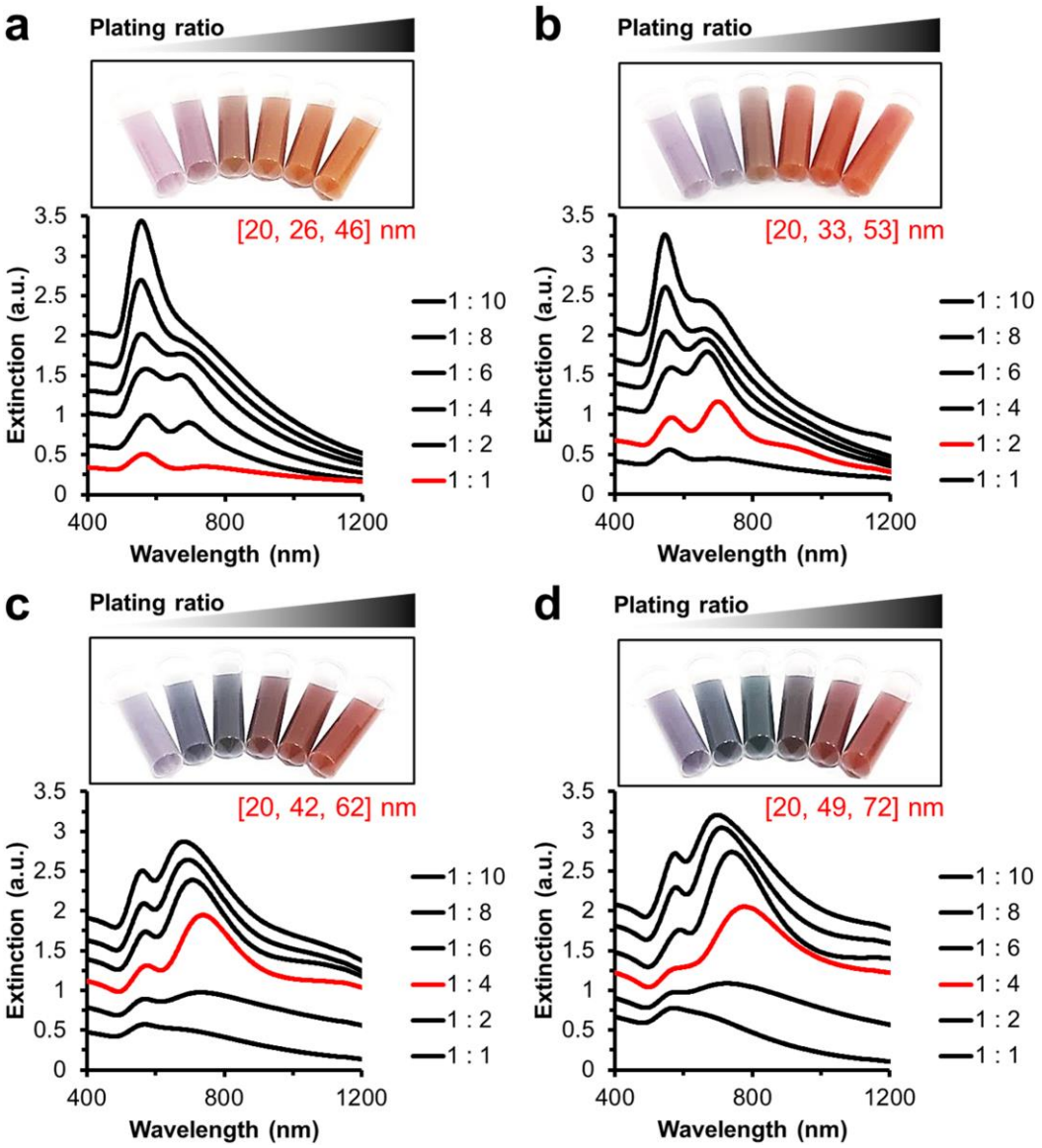

Fig. S14 Characterization of PDA-based Au NMs (Au@PDA@Au NPs) with four defined interior nanogap thicknesses. (a)–(d) The plasmonic properties of Au@PDA@Au NPs obtained by using different plating ratios for each nanogap size were monitored by UV-vis-NIR spectrophotometry. The plating ratios shown in the figure legends refer to the volume ratios between the Au@PDA@Seed NPs and the plating solution. In each panel, red text indicates the internal radii (represented by [r_1, r_2, r_3]) of the Au NMs formed by using the optimal plating ratio that gives rise to the most red-shifted subradiant plasmon resonance peak in the near-infrared (NIR) region (red).[5] Inset: Color of Au NMs obtained with increasing plating ratios (from left to right).

Internal radii [r_1, r_2, r_3] (nm)[a]	Superradiant plasmon resonance peak (nm)	Subradiant plasmon resonance peak (nm)	Hydrodynamic diameter (PDI) (nm)[b]
[19.5 ± 1.0, 26.1 ± 2.8, 46.2 ± 3.5]	558	783	99.4 ± 0.7 (0.172)
[19.5 ± 1.0, 32.8 ± 2.6, 52.9 ± 3.0]	565	699	112.5 ± 1.2 (0.153)
[19.5 ± 1.0, 41.7 ± 3.4, 62.4 ± 3.4]	574	738	124.6 ± 1.6 (0.169)
[19.5 ± 1.0, 49.0 ± 2.2, 71.8 ± 1.9]	N.D.[c]	775	152.8 ± 1.5 (0.120)

Table S8 Physicochemical characterization of the optimized PDA-based Au NMs with four defined interior nanogap thicknesses. [a]Values were obtained from the analysis of over 50 particles in multiple TEM images by the ImageJ software. Results are given in mean ± SD. The physical dimension of the optimized Au NSs is represented by [r_1, r_2, r_3],[5] where r_1 indicates the radius of the Au core, r_2 indicates the radius of the Au@PDA NP, and r_3 indicates the radius of the whole Au@PDA@Au NP. [b]Measured by the ZetaPlus zeta potential and particle size analyzer. Results are given in mean ± SD of 10 measurements. Numeral in bracket indicates PDI. [c]"N.D." refers to any surface plasmon resonance peak not detectable by the UV-vis-NIR spectrophotometer.

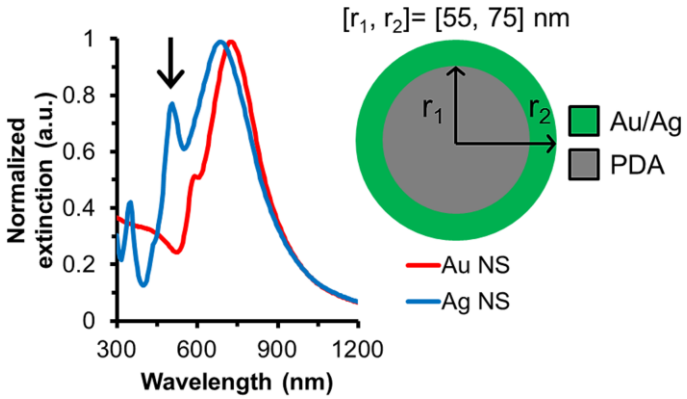

Fig. S15 Calculated extinction spectra of PDA-based Au NS and Ag NS with fixed internal radii [r_1, r_2] of [55, 75] nm. In all calculations, the refractive index of all PDA cavities is set as 1.7. In the NIR region, the plasmon peaks originating from the coupling of the metal shell of Au NS (685 nm) and Ag NS (725 nm) do not deviate much in terms of extinction and peak sharpness, except that Ag NS exhibits a λ_{spr} in higher energy. However, in the visible region, Ag NS displays a more pronounced λ_{spr} located at 505 nm (arrow) than Au NS does. Note that the λ_{spr} at 350 nm is the bulk peak of Ag.

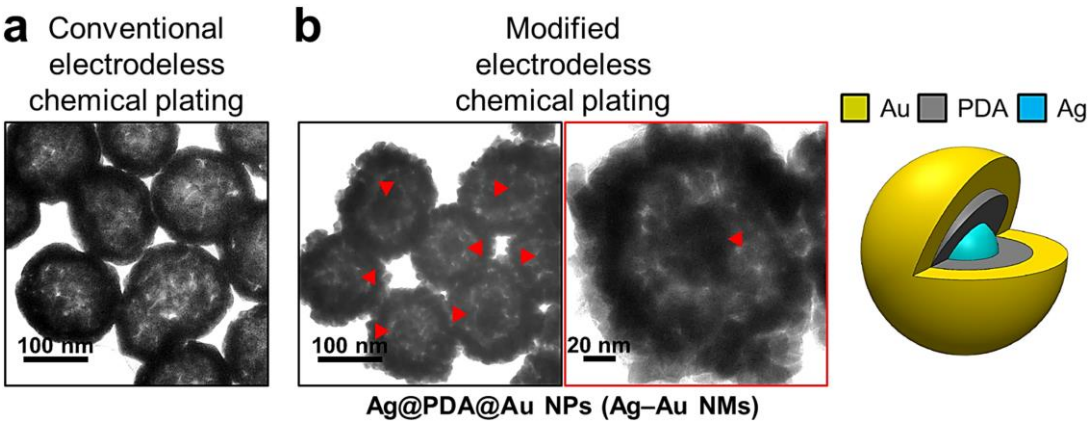

Fig. S16 Characterization of PDA-based bimetallic Ag–Au NMs (Ag@PDA@Au NPs) constructed by two different plating methods. (a) By using the conventional method of electrodeless chemical plating, we observed by TEM imaging that the Ag cores are etched away by the Au^{3+} present in the plating solution due to galvanic replacement. (b) In our modified approach,[8] we intentionally lowered the oxidizing power of the Au^{3+} by simultaneously (1) increasing the pH value of the plating solution to ~11 and (2) slowing down the injection rate of the modified plating solution to 0.02 mL/min as controlled by a syringe pump. TEM imaging reveals the improved fabrication of Ag–Au NMs with intact Ag cores (triangles), free of galvanic replacement. However, the resultant Au NS around the Ag core is evidently rougher than those of Au NSs (Fig. 2d) and Au NMs (Fig. 3d) shown in the main text.

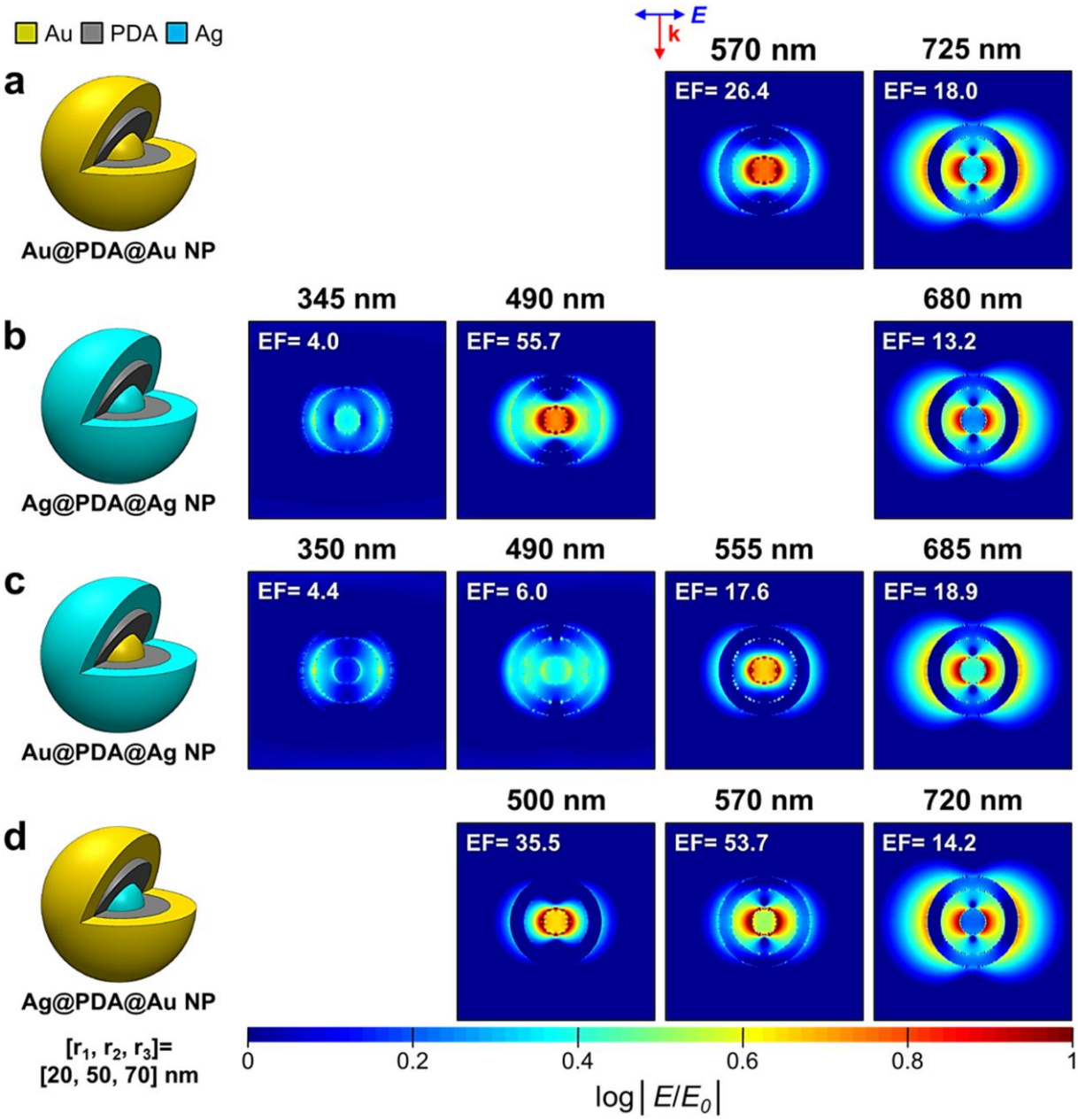

Fig. S17 Simulated electric field intensity distribution of polydopamine-based NMs with fixed internal radii [r_1, r_2, r_3] of [20, 50, 70] nm. For each kind of NM, including (a) Au@PDA@Au NP (Au NM), (b) Ag@PDA@Ag NP (Ag NM), (c) Au@PDA@Ag NP (Au–Ag NM), and (d) Ag@PDA@Au NP (Ag–Au NM), simulated electric field intensity distribution ($\log|E/E_0|$) obtained at each indicated λ_{spr} is shown. EF denotes the calculated local field enhancement factor (i.e., E/E_0). In all calculations, the refractive index of all PDA cavities is set as 1.7. We observed that introduction of a Ag core inside the NM results in strong local field enhancement in the visible region (between 490 and 570 nm). However, variation in the metallic composition of the outer NS does not result in any significant change in electric field distribution of the four NMs, especially in the NIR region (beyond 650 nm).

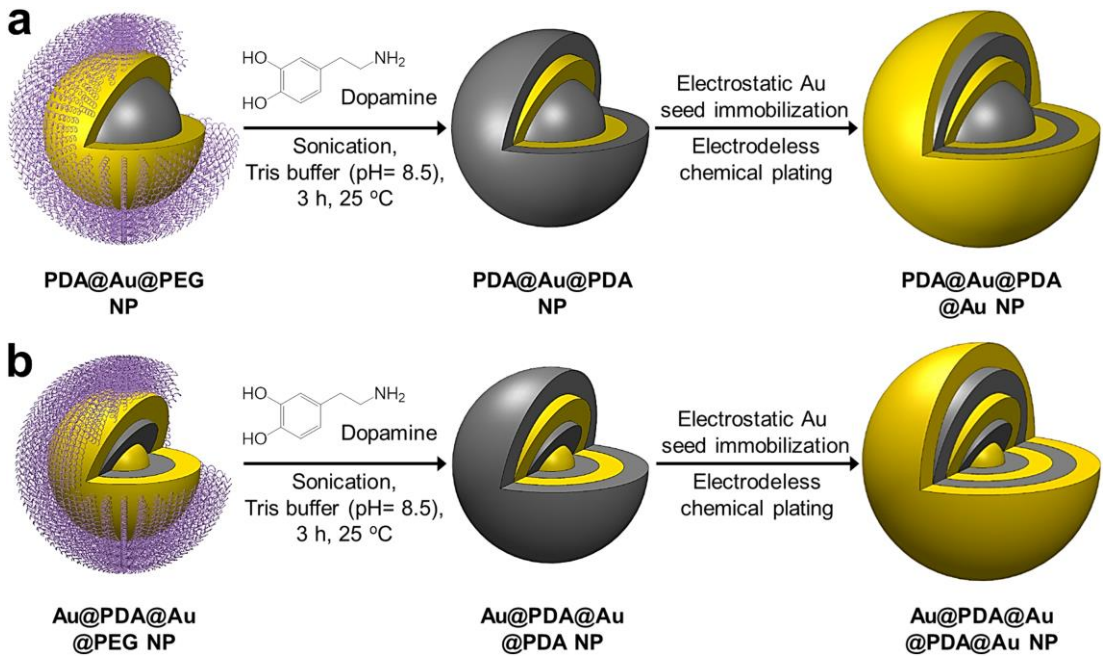

Fig. S18 Schematic illustration of the bottom-up "layer-by-layer" assembly of PDA-based concentric Au NSs with a (a) four-layered structure (without a Au core, PDA@Au@PDA@Au NP) and (b) five-layered structure (with a Au core, Au@PDA@Au@PDA@Au NP).

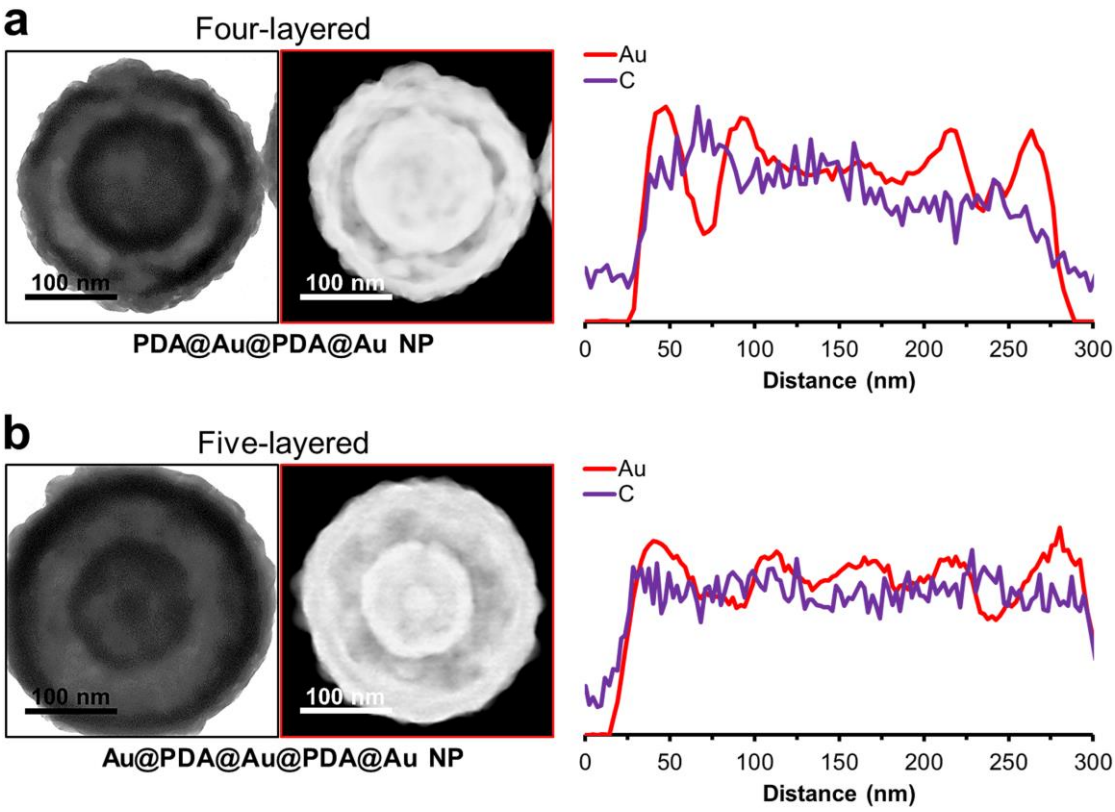

Fig. S19 Structural characterization of PDA-based concentric Au NSs with a (a) four-layered structure (without a Au core, PDA@Au@PDA@Au NP) and (b) five-layered structure (with a Au core, Au@PDA@Au@PDA@Au NP). Left panel: Single-particle TEM images taken in both bright-field and dark-field modes. Right panel: Elemental line mapping of the corresponding NP as shown in the left panel clearly reveals its elemental composition and structural profile.

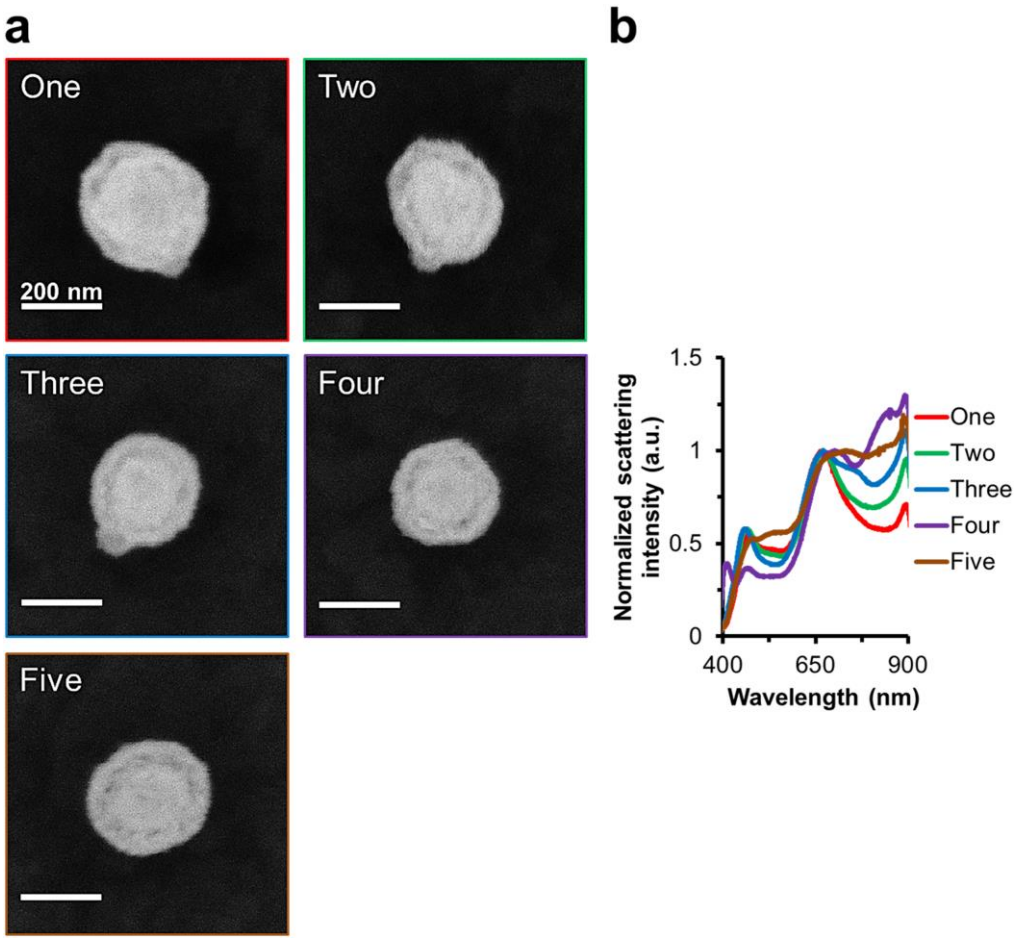

Fig. S20 Single-particle dark-field scattering spectroscopy of PDA-based concentric Au NSs with a four-layered structure (PDA@Au@PDA@Au NPs). (a) Single-particle scanning electron microscopic (SEM) images of five individual PDA@Au@PDA@Au NPs acquired by a backscattered electron (BSE) detector. (b) Scattering spectra recorded for each of the single NP shown in (a). Our observation wavelength window (i.e., 400–900 nm) is limited by the charge-coupled device (CCD) camera used in the measurements. All scattering signals are normalized against the highest plasmon resonance peak existing in this window to prevent interference from the noise detected at the two wavelength extremes (i.e., 400 nm and 900 nm).

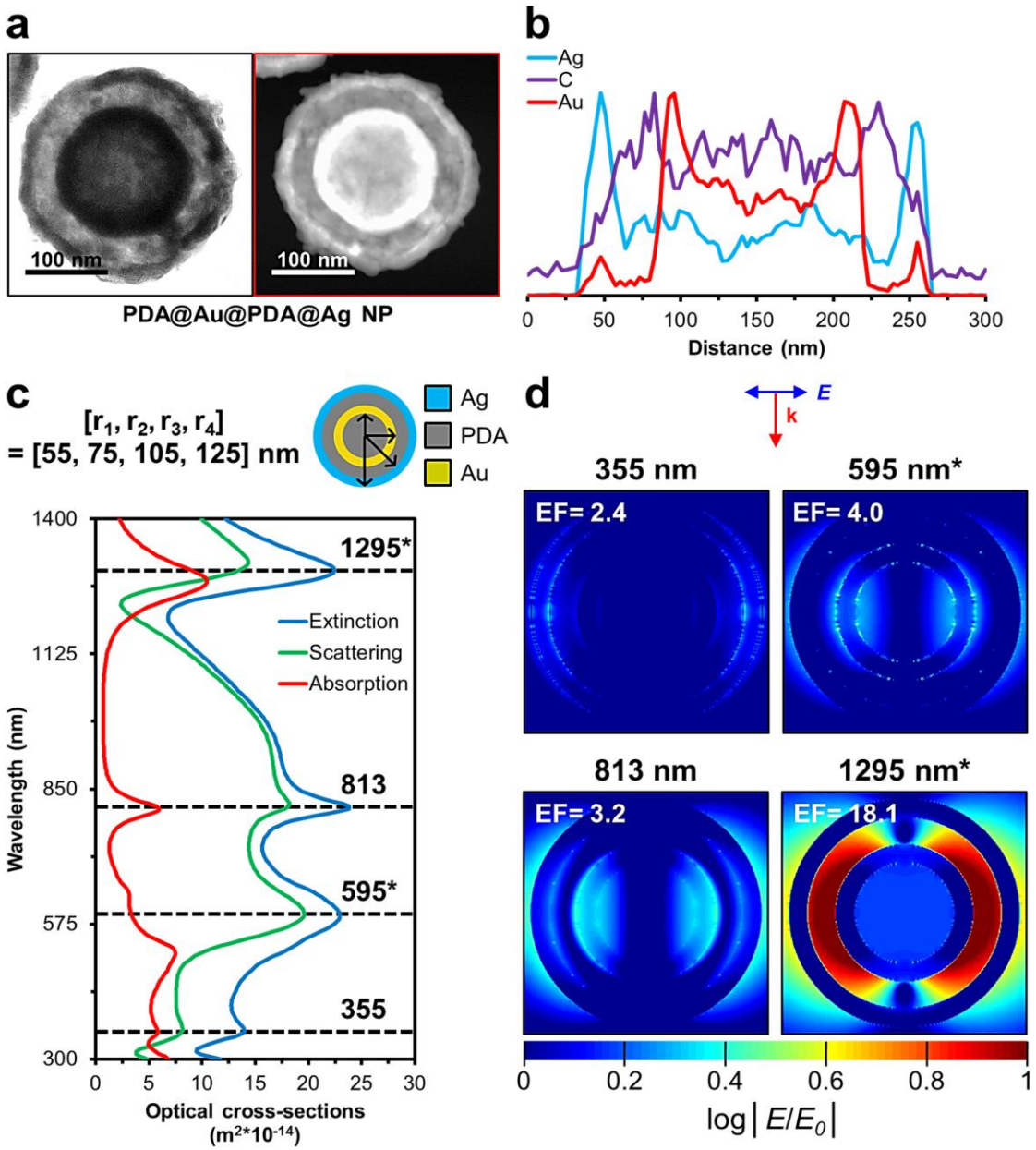

Fig. S21 Structural characterization and plasmonic properties of PDA-based bimetallic concentric Au–Ag NSs with a four-layered structure (PDA@Au@PDA@Ag NPs). (a) TEM image of a PDA@Au@PDA@Ag NP taken in both bright-field and dark-field modes. (b) Elemental line mapping of the corresponding NP shown in (a) clearly reveals its elemental composition and structural profile. (c) Optical cross-sectional spectra of an ideal PDA@Au@PDA@Au NP with fixed internal radii [r_1, r_2, r_3, r_4] of [55, 75, 105, 125] nm. Surface charge distribution contour obtained at each indicated λ_{spr} is included. All Fano resonance modes are marked by an asterisk (*). (d) Simulated electric field intensity distribution ($\log|E/E0|$) obtained at each indicated λ_{spr}. EF denotes the calculated local-field enhancement factor. In all calculations, the refractive index of all PDA cavities is set as 1.7.

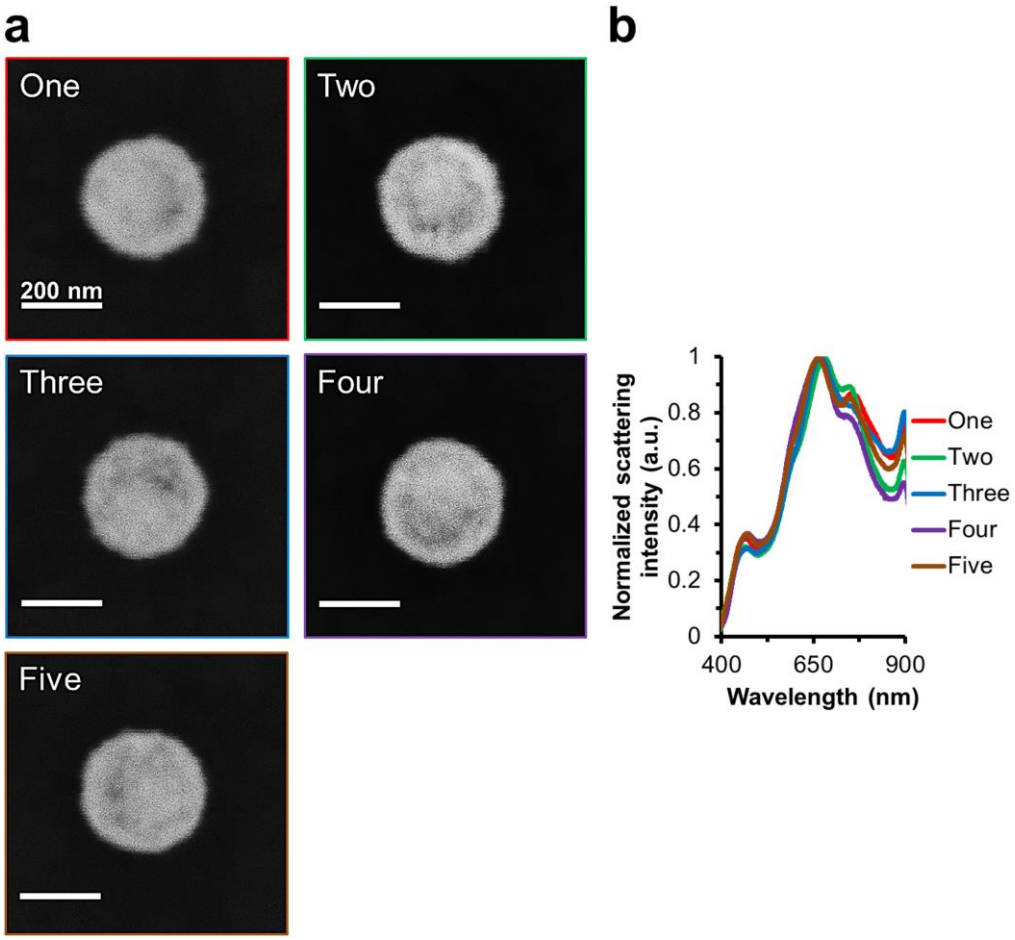

Fig. S22 Single-particle dark-field scattering spectroscopy of PDA-based concentric Au NSs with a five-layered structure (Au@PDA@Au@PDA@Au NPs). (a) Single-particle SEM images of five individual Au@PDA@Au@PDA@Au NPs acquired by a BSE detector. (b) Scattering spectra recorded for each of the single NP shown in (a). Our observation wavelength window (i.e., 400–900 nm) is limited by the CCD camera used in the measurements. All scattering signals are normalized against the highest plasmon resonance peak existing in this window to prevent interference from the noise detected at the two wavelength extremes (i.e., 400 nm and 900 nm).

Sample	(a) Nanoshells		(b) Nanomatryoshkas				(c) Concentric nanoshells		
	PDA @Au NP	PDA @Ag NP	Au @PDA @Au NP	Ag @PDA @Ag NP	Au @PDA @Ag NP	Ag @PDA @Au NP	PDA @Au @PDA @Au NP	PDA @Au @PDA @Ag NP	Au @PDA @Au @PDA @Au NP
Experiment (nm)	590	370	580	426	N.D.[a]	N.D.[a]	636	404	668
Theory (nm)	N.D.[a]	350	570	345	350	500	617	355	626
Experiment (nm)	779	N.D.[a]	775	N.D.[a]	427	N.D.[a]	915	N.D.[a]	830
Theory (nm)	725	505	725	490	490	570	833	595	799
Experiment (nm)		712		757	547	638	N.D.[a]	958	1359
Theory (nm)		685		680	555	720	1304	813	1260
Experiment (nm)					755			N.D.[a]	
Theory (nm)					685			1295	

Table S9 Summary of the optical properties of PDA-based plasmonic (a) nanoshells, (b) nanomatryoshkas, and (c) concentric nanoshells. [a]"N.D." refers to any surface plasmon resonance peak not detectable by the UV-vis-NIR spectrophotometer.

Supporting References

1 Q. Liu, B. Yu, W. Ye and F. Zhou, *Macromol. Biosci.*, 2011, **11**, 1227–1234.
2 B. Yu, J. Liu, S. Liu and F. Zhou, *Chem. Commun.*, 2010, **46**, 5900–5902.
3 N. R. Jana, L. Gearheart and C. J. Murphy, *J. Phys. Chem. B*, 2001, **105**, 4065–4067.
4 J. B. Jackson and N. J. Halas, *J. Phys. Chem. B*, 2001, **105**, 2743–2746.
5 C. Ayala-Orozco, C. Urban, M. W. Knight, A. S. Urban, O. Neumann, S. W. Bishnoi, S. Mukherjee, A. M. Goodman, H. Charron, T. Mitchell, M. Shea, R. Roy, S. Nanda, R. Schiff, N. J. Halas and A. Joshi, *ACS Nano*, 2014, **8**, 6372–6381.
6 X. Liu, J. Cao, H. Li, J. Li, Q. Jin, K. Ren and J. Ji, *ACS Nano*, 2013, **7**, 9384–9395.
7 C. K. Choi, J. Li, K. Wei, Y. J. Xu, L. W. Ho, M. Zhu, K. K. To, C. H. Choi and L. Bian, *J. Am. Chem. Soc.*, 2015, **137**, 7337–7346.
8 M. Yang, Z. D. Hood, X. Yang, M. Chi and Y. Xia, *Chem. Commun.*, 2017, **53**, 1965–1968.